Bull. Mater. Sci., Vol. 35, No. 3, June 2012, pp. 357–364. © Indian Academy of Sciences.

Property change during nanosecond pulse laser annealing of amorphous NiTi thin film

S K SADRNEZHAAD*, NOUSHIN YASAVOL†, MANSOUREH GANJALI†† and SOHRAB SANJABI†

Centre of Excellence for Advanced Materials, Department of Materials Science and Engineering, Sharif University of Technology, Tehran, Iran

†Department of Materials, Tarbiat Modares University, Tehran, Iran

††Department of New Materials, Materials and Energy Research Centre, Karaj, Iran

MS received 11 February 2011; revised 1 September 2011

Abstract. **Nanosecond lasers of different intensities were pulsed into sputter-deposited amorphous thin films of near equiatomic Ni/Ti composition to produce partially crystallized highly sensitive *R*-phase spots surrounded by amorphous regions. Scanning electron microscopy having secondary and back-scattered electrons, field emission scanning electron microscopy, optical microscopy and X-ray diffraction patterns were used to characterize the laser treated spots. Effect of nanosecond pulse lasering on microstructure, morphology, thermal diffusion and inclusion formation was investigated. Increasing beam intensity and laser pulse-number promoted amorphous to *R*-phase transition. Lowering duration of the pulse incidence reduced local film oxidation and film/substrate interference.**

Keywords. **SMA; NiTi; pulse laser; thin film; crystallization.**

1. Introduction

NiTi possesses a series of interesting properties like ability to recover large transformation work, high actuation/weight ratio, shape recovery, damping capacity, chemical resistance, biocompatibility and pseudoelasticity (Fua *et al* 2004; Shaw and Crone 2004). Its microstructure and properties are, however, drastically sensitive to composition, thermomechanical treatment, heat evolution and prevailing stable and/or pseudo-stable phase presence (Busch and Johnson 1991; Ishida *et al* 1995; Zhang *et al* 2003; Ni *et al* 2005; Zhan *et al* 2006). Fast response, instant actuation and precise control of deformation and force are ideal capabilities anticipated from microelectromechanical systems (MEMs). In order to achieve these features, a small thermal hysteresis is most desirable. Nearly all NiTi martensitic transformations associate with wide temperature hysteria. The rhombohedral (*R*-phase) transition of the NiTi shape memory alloy (SMA) exhibits, however, a small thermal hysteresis of 1·5 °C which makes it desirable for delicate functional uses.

Due to fast sensing power and high actuation speed, NiTi thin films can be used in elegant applications like microsensors, light valves, nerve clamps, microelectrodes, microwrappers, microvalves, micropumps, invasive instruments, actuated microendoscopes, implantable drug delivery devices, nanoscale shape memory actuators, sensor microarray for infrared radiation and on-off optical switches of spatial light modulators (Kohl *et al* 1999, 2000; Seguin *et al* 1999; Makino *et al* 2000; Takeuchi and Shimoyama 2000; Luskin and Palmstrom 2004; Wang *et al* 2005; Zamponi *et al* 2007; Chan *et al* 2008; Wood *et al* 2008). NiTi thin plates are generally made by physical vapour deposition because of weak workability of NiTi cast SMAs (Bellouard *et al* 1999; Xu *et al* 2006; Bellouard 2008). High-intensity laser treatment results in fast heating/cooling processes which retard martensite formation by promotion of the non-perpendicular lattice inversion. Crystallization into high-temperature austenitic (B2) phase results in thin-film property change. Thermal defects caused by frequent heating/cooling cycles are not desirable because of the unwanted influence on transformation temperatures which results in the malfunction of the manufactured microelectromechanical systems (MEMs) (Xu *et al* 2006).

Pulse lasering results in faster actuation response than conventional furnace annealing or continuous wave (CW) laser-treatment (Krishna *et al* 2007; Birnbaum *et al* 2008; Clare *et al* 2008). Selective laser melting has, for example, resulted in formation of a high aspect ratio and a three-dimensional NiTi microelectromechanical compartment as reported in earlier studies (Krishna *et al* 2009; Sadrnezhaad *et al* 2009; Zanotti *et al* 2009). Advantage of laser annealing is development of a biasing force which results in a back-to-preliminary-state tendency not achievable in traditional heat treatment processes. Laser heating results in formation of thermoelastic crystalline areas surrounded with wide amorphous regions exploitable in design of many functional systems (Fua *et al* 2004). Furnace cooling can decrease the residual stresses that may remain throughout the layer (Xu *et al* 2006).

*Author for correspondence (sadrnezh@sharif.edu)

Two-way shape memory effect is highly desirable in manufacture of the MEMs (Chan *et al* 2008). In continuous wave (CW) lasering, partially crystallized boundaries usually form between amorphous and fully crystallized regions. These boundaries slow down the response of the actuators. They look omissible, however, by use of the pulse lasering treatment (Xu *et al* 2006). Instant pulse-mode treatment looks capable to reduce the thermal diffusion of the constituents across thin film towards holding substrate (Xu *et al* 2006). Precise control of the pulse lasering conditions can help attain the projected crystallization and the subsequent growth courses of action (Xu *et al* 2006).

Based on the above discussion, laser parameters can be of help in microstructural development of MEMs. SMA sensation/actuation behaviour can substantially change by intensity and width of laser irradiation (Chan *et al* 2008). Lowering duration of the laser incidence diminishes the NiTi oxidation (Sanjabi *et al* 2005). Martensitic transformation dramatically relates to the layer composition. This composition can strongly change by extended thermal diffusion. Intensive lasering can impinge on the response-time of the actuator (Wang *et al* 2004). Micro-actuator design is favoured by recoverable stresses, large transformation strains and frequent and fast counteractions. NiTi thin films inheriting the *R*-phase structure propose desirable functional behaviours applicable to the newly made micro-actuator systems (Bellouard 2008).

The purpose of this study is to shed some light on the local *R*-phase crystallization behaviour of the sputtered amorphous NiTi layers irradiated with nanosecond pulsing lasers. The goal of the study is to optimize laser intensity, the pulse number and the incidence duration for obtaining the most appropriate crystallized spots surrounded by wide amorphous neighbours. The distinction between submicron microstructure of the nanosecond pulse laser spots obtained from nanosecond laser treatment with the austenite–martensite morphology of the previously observed millisecond pulse laser treatment (Sadrnezhaad *et al* 2009) will be elucidated.

2. Experimental

NiTi thin films of $\sim$2 μm thickness were deposited on silicon wafer (100) plane by co-sputtering from separate elemental Ni and Ti targets according to the procedure explained in an earlier work (Birnbaum *et al* 2009). NiTi crystallized microstructure was induced by a single-pulse *Q* switched Nd:YAG laser of 1064 nm wavelength with mainly harmonic near-Gaussian beam profile. Duration of the pulse was 10 ns and the beam diameter was 1 mm. The position of the specimen was adjusted by *X*–*Y*–*Z* stage having an accuracy of 0·1 μm.

Pulse lasering was under atmospheric condition with an intensity of 2 to 70 $\pm$ 1 mJ/mm^2 which was measured by a profilometer, as listed in table 1. Near Gaussian laser beam producing round spots with different radii in perpendicular transverse directions was used to heat up different locations on the layers. Microstructures of the spots were studied by optical microscopy (OM) using polarized light produced by ND12 and NIC Olympus filters, field-emission scanning electron microscopy (FESEM) and scanning electron microscopy (SEM) with secondary electron (SE) and back-scattered electron (BSE) detectors. In order to measure the compositional changes of the crystallized area against laser intensity, spot mapping was attained. Local analyses of the amorphous and laser crystallized layers were determined by X-ray diffraction (XRD) using CuKα, 40 kV, 40 mA (Philips Xpert, The Netherlands). Each data point resulted from four separate measurements.

3. Results and discussion

A typical spot produced by near Gaussian pulse lasering of the sputtered amorphous film is demonstrated in figure 1. Microstructure of the spot is clearly distinguishable from the unlasered amorphous regions. Distinct boundaries separating the irradiated spots from the amorphous layers are observable in optical micrographs as shown in figures 1 and 2. Near the boundary, a wrinkled region is clearly observable in figure 2b which reveals thermal stresses caused by laser irradiation. No sign of crystallization in the central parts of the spots are observed in figure 2. Similar observations have previously been reported by other researchers (Chan *et al* 2008).

Figure 2 compares the optical images of thin film irradiated with pulse laser beams of 2, 20, 30, 40 and 50 mJ/mm^2 intensities with the as sputtered NiTi layer. At lower intensities, swelling of the layers due to pulse lasering is observable (figure 2b). Hilly-like texture of this figure indicates that at a mJ/mm^2, pulse cannot produce sufficient heat for shear-transition of the amorphous layer. Larger intensities result in greater thermal expansion and miniature excitation of the atoms to separate from each other. At 5 mJ/mm^2, a few islands of the *R*-phase are formed on the lasered section (figure 2c). Expansion of the *R*-phase region seems to cause larger thermal strains at higher laser powers of 30, 40 and 50 mJ/mm^2 as shown in figures 2d, e and f. The exemplified morphologies reveal that the intensities larger than 20 mJ/mm^2 can create enough thermal power for crystallization of a substantial portion of the amorphous layer.

Table 1. Voltage and intensity of laser beam pulsed on NiTi amorphous thin film.

Applied voltage (kV)	0·98	0·99	1·00	1·01	1·02	1·03	1·04	1·05	1·07	1·15	1·23	1·33	1·45	1·50	1·60
Laser intensity (mJ/mm^2)	2·0	2·8	4·0	4·5	5·8	6·3	7·5	9·5	13·0	20	30	40	55	60	70

Because of very short (nanosecond) incident, no precipitation of the intermetallic phases is observable in the lasered regions. By increasing the laser intensity, thickness of the *R*-phase bands in the marginal zones of the crystallized region grows (figures 2e and f). In addition to the *R*-phase, thermally shocked stress-induced martensitic bands are also observable in the marginal zones of the crystallized spots produced by large intensity lasers (figure 3). Figure 3b indicates fine martensitic locations of a typically pulsed spot at a laser intensity of 55 mJ/mm^2. Higher laser intensities cause greater quenching rates which result in formation of higher strained martensitic lattice distortion (Birnbaum *et al* 2009).

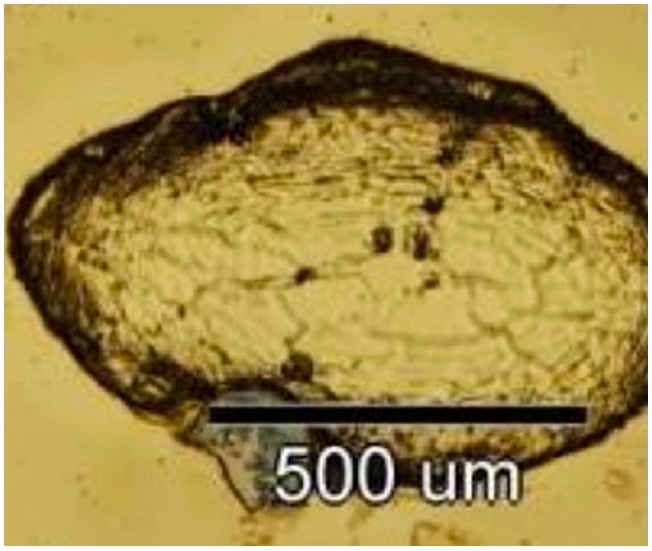

Figure 1. Optical microstructures of a typical spot produced by nanosecond pulse laser irradiation of NiTi amorphous thin layer at an intensity of 25 mJ/mm^2.

Near Gaussian intensity profile of the laser beam results in a temperature gradient perpendicular to the laser track (Chan

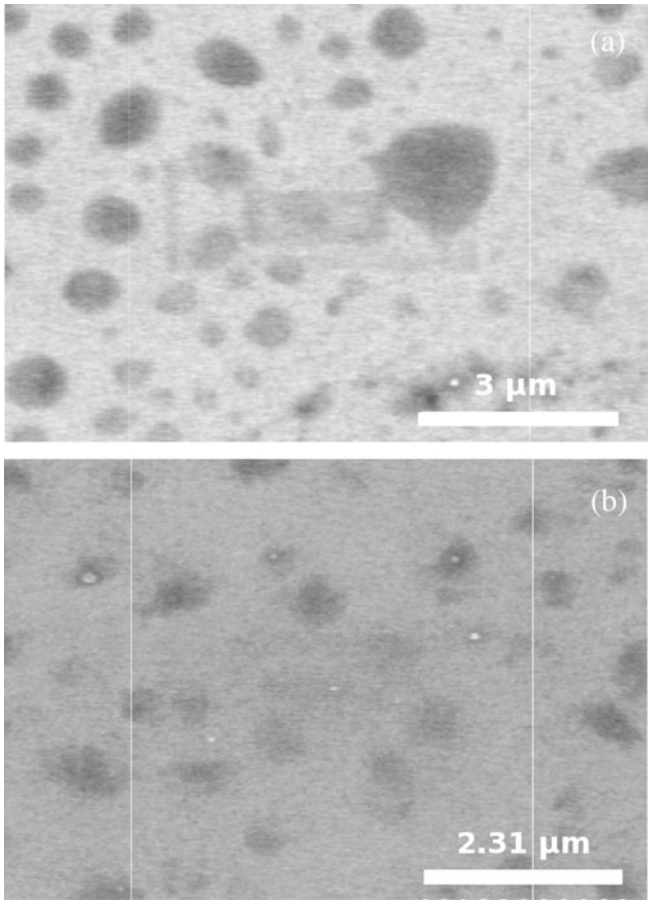

Figure 3. FESEM images of spots lasered at intensities of (**a**) 40 and (**b**) 55 mJ/mm^2.

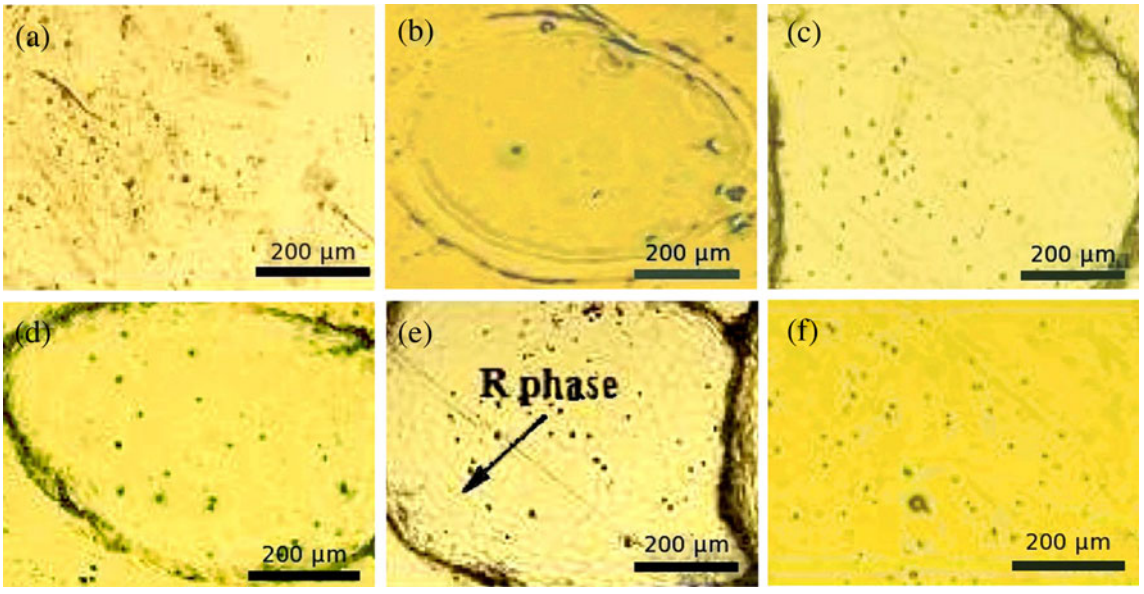

Figure 2. Effect of PLA on optical microstructure of NiTi thin film: (**a**) as sputtered and (**b** to **f**) irradiated with pulse laser beam of 2, 20, 30, 40 and 50 mJ/mm^2 respective intensities.

et al 2008). Existence of martensite and *R*-phase in the margins of the annealed spot implies that rapid cooling during laser processing can cause retention of the amorphous phase in the central part of the annealed region (Zamponi *et al* 2007; Sadrnezhaad *et al* 2009).

Laser intensities of 2 and 5 mJ/mm^2 produce no special texture in the amorphous layer; while a number of dark specks appear at intensities of 40 and 55 mJ/mm^2 as observable in figures 2 and 3. FESEM images shown in figure 3 indicate that enhancement of the laser intensity reduces the number but expands size of the dark specks. Formation of these specks seems due to the substrate/film interactions resulting in expectable shape memory destruction and actuation capability diminution. Investigating the laser-treated thermal-diffusion zones seems hence an impressive research goal.

Heating depth of the pulsed laser annealing (PLA) zone can be evaluated from the following simple equation (Ivakin *et al* 2004):

$$L \approx 4(Dt)^{1/2}, \quad (1)$$

where L is the depth of heating, D the thermal diffusivity and t the pulse duration. For exposure time of 10 ns, designated alloy composition of $Ni_{50}Ti_{50}$ and respective thermal diffusivities of Ni and Ti being 23 and 7 mm^2/s (Ifflander 2001), the depth of the heated zone is estimated to be 2·45 μm. This is greater than 2 μm film thickness, implying that the induced laser not only heats the amorphous layer, but can also diffuse into the holding substrate. Since the thermal diffusivity of the film rises with temperature, it is expected that the depth of the heated zone exceeds 2·45 μm during each laser pulse irradiation. Laser-induced heating results, therefore, Ni/Ti interactions take place with Si at the film/substrate interface. Although this can result in a stronger adherence of the thin film to the substrate, adjustment of the laser intensity or utilization of a buffer layer may eliminate thin film/Si substrate interference at the interface region (Grummon *et al* 1999).

A number of white inclusions produced at 40 and 55 mJ/mm^2 intensities are also observed in figure 3. The inclusions present in figure 3a are, however, much smaller than those in figure 3b. According to the literature, these are metal silicides formed by reaction of silicon with nickel and titanium constituents of the thin layer (Gill *et al* 2002; He *et al* 2005). Further experiments show that using intensities of 60 and 70 mJ/mm^2 causes the formation of large and copious inclusions. Merger of small inclusions at high intensities is also possible. Formation of too many inclusions results in change of the composition and reduction of the *R*-phase in the interface regions (Birnbaum *et al* 2009).

Figure 4 shows geometric perceptions of two inclusions created at intensities of 55 and 60 mJ/mm^2 by PLA treatment. The first rectangle-like inclusion has 988 × 1753 nm^2 area and 39·14 atom % silicon, 32·37 atom % titanium and 28·49 atom % nickel which correspond to $Si_{1.4}Ti_{1.1}Ni$ chemical composition. The second triangle-like inclusion has 5·7 μm height and 65·55 atom % silicon, 18·93 atom % titanium and 15·52 atom % nickel which correspond to $Si_{4.2}Ti_{1.2}Ni$ chemical composition. The increasing composition of silicon by intensity of the laser approves the thin film/substrate interference at heat affected interface zones.

Previous researchers have indicated that the activation energy for crystallization of the sputtered NiTi films is less than that for bulk NiTi alloy (Chan *et al* 2008). Crystallization of the former was expected, hence, was found to be much easier than the latter (Chan *et al* 2008). The sputtered film builds up, however, cracks are formed when intense lasering is attained (Takeuchi and Shimoyama 2000). Figure 5 illustrates crack formation in the areas crystallized by the pulse lasering of the film at an intensity of 40 mJ/mm^2. Considerable differences in the coefficients of thermal expansion of NiTi with silicon and silicon nitride with a ratio of about 4 (Ifflander 2001; Ivakin *et al* 2004) promote crack formation in thin layer. FESEM images of PLA region shown in figure 6 illustrate crack origination from the holes generally created by sputtering of thin films and extension towards the

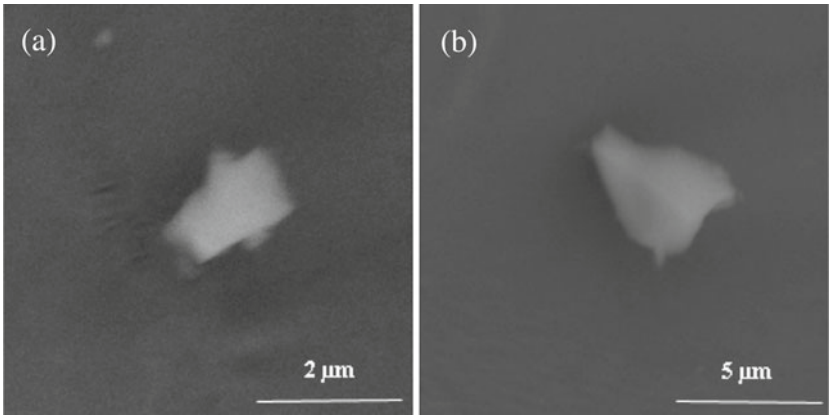

Figure 4. SEM images of an inclusion captured with BSE detector on surface of a spot lasered at intensities of (**a**) 55 and (**b**) 60 mJ/mm^2.

crack-less zones. Nanosecond pulse laser annealing seems, however, to retain holes from initiation of thermal expansion cracks.

Spot analysis reveals that silicon uptake makes composition of the layer uneven. Composition variation is also caused by instability of the pulse frequency and the laser near-Gaussian beam profile. To eliminate the error caused by ignoring of the thermal diffusion zone (Chan *et al* 2008), nanosecond pulse lasering can be used as a simple operative approach. Much higher absorption coefficient of Ni compared with Ti for Nd:YAG laser energy (Ifflander 2001) causes faster Ni diffusion towards the film/substrate interface and creation of an uneven composition (table 2). Another advantage of the nanosecond pulse lasering is the reduction of the laser/film interaction time which reduces film oxidation. Small amounts of the remaining oxygen may, however, dictate some oxidation.

Figure 7 shows optical microstructure of PLA NiTi amorphous film as a function of intensity and the number of pulsed laser. A greater pulse number results in more extensive crystallization, the greater *R*-phase formation and the extension to the spot centre of the heat effect. A single pulse can result in mere *R*-phase formation at marginal areas of thin layer. The inset of the figure illustrates the safe *R*-phase formation conditions together with the laser intensity and pulse number effects on cracking and ablation of the NiTi thin film samples.

Figure 5. Optical micrographs showing crack propagation in amorphous NiTi thin layer caused by 40 mJ/mm^2 PLA.

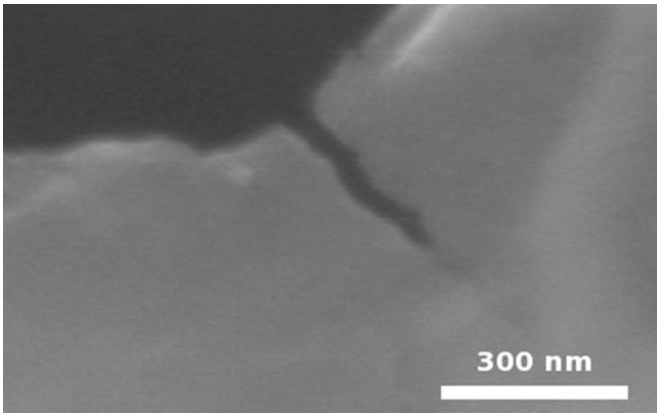

Figure 6. FESEM image of a crack started from a sputtering hole and propagated at 60 mJ/mm^2 laser intensity.

Table 2. Analysis of PLA spots located on amorphous NiTi thin film determined by SEM EDS.

Laser intensity (mJ/mm^2)	Position (50×50 µm^2)	Elemental composition (atom %)			
		Ni	Ti	Si	O
13	Middle	47·99	51·54	0·47	0
	Centre	47·16	52·68	0·16	0
20	Middle	48·62	51·32	0·06	0
30	Boundary	49·61	50·39	0	0
	Middle	50·13	54·01	0·03	
	Centre	45·08	51·11		3·81
40	Boundary	41·02	44·32	0·03	14·28
	Middle	45·55	50·74	3·08	–
	Centre	47·91	52·18	0·01	0·01
	Precipitates zone	46·37	51·72	0·06	1·29
55	Boundary	45·49	49·79	0·14	4·58
	Middle	47·88	52·12	0	–
	Centre	47·20	50·65	0	2·15
60	Boundary	47·89	51·49	0·61	0
	Middle	48·48	51·36	0·16	0
	Centre	48·18	50·73	1·09	0
70	Boundary	45·99	49·64	0·42	3·95
	Middle	48·45	51·55	0	0
	Centre	47·93	52·07	0	0

Figure 8 shows BSSEM micrographs of a single and a triple pulse spot having produced the *R*-phase. At constant intensity, increasing of the pulse number promotes crystallization towards the spot centre. Multi-pulsed laser irradiation causes domination of the rhombohedral NiTi phase. This is assessed by XRD peak analysis and SEM microstructural images. The *R*-phase formation seems due to the residual thermal stresses retained after lasering treatment. In multi-pulsed areas of PLA, each pulse induces a certain amount of shock onto the amorphous layer which promotes the *R*-phase formation by the insertion of the internal stresses. Single pulse laser irradiation demonstrates that just in the margin of the PLA spot, where wrinkles are observed, the *R*-phase formation is favourably promoted by the stress rather than the sole heating effect. Higher number of pulses on thin film results in crack-propagation both within the inner area of the crystallization domain as well as throughout the laser spotted regions. Escalation up to 7 or 9 of the number of pulses causes ablation. With laser energy enhancement to 18 mJ/mm^2, the trend becomes repetitive with a higher speed.

Figure 9 contains XRD spectrum of thin film spot irradiated at room temperature. It confirms that the crystallization has occurred. Small *R*-phase peaks at $2\theta = 42{\cdot}3$ and 42·9 correspond to (112) and (300) crystallographic planes,

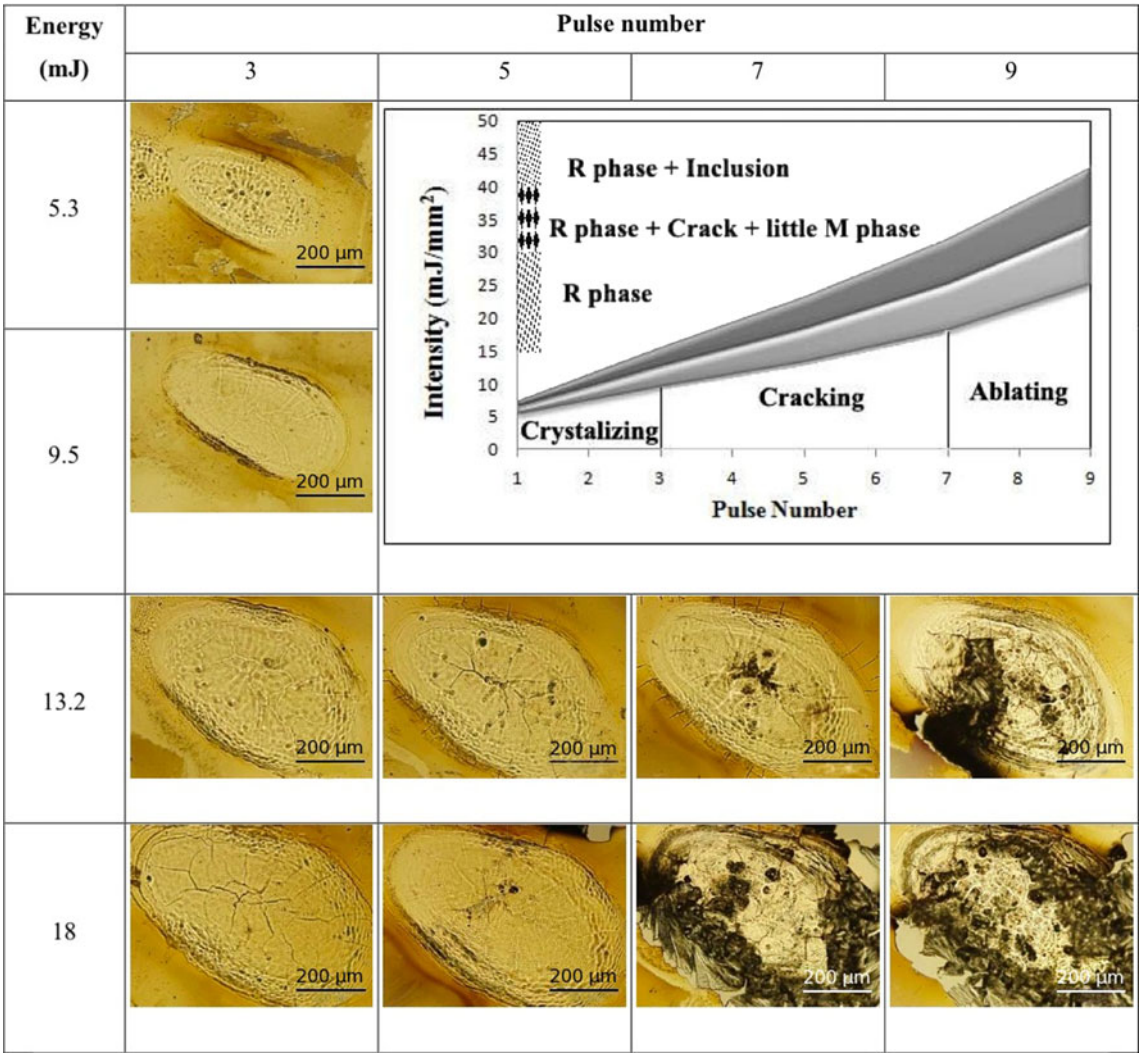

Figure 7. Optical micrographs of NiTi amorphous thin film lasered at intensity and pulse numbers indicated in figure. Inset of figure illustrates safe *R*-phase formation conditions together with laser intensity and pulse number effect on cracking and ablation of NiTi thin film samples.

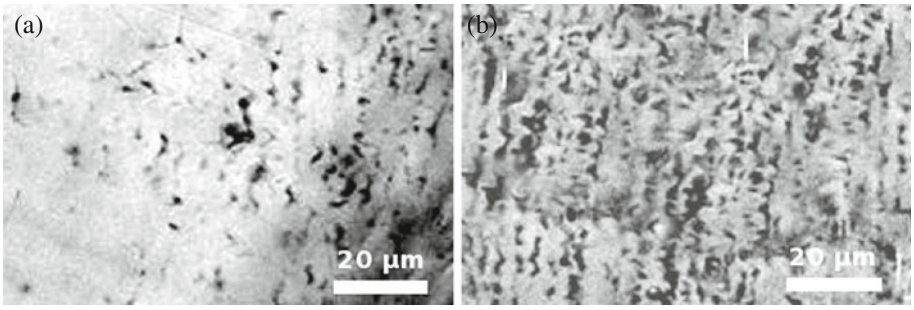

Figure 8. Back scattered SEM images of *R*-phase regions formed by 13·2 mJ/mm^2 laser intensity pulsed: (**a**) only once and (**b**) three times.

respectively (Birnbaum *et al* 2009). Incrementing the laser energy increases intensities of these peaks and reveals other *R*-phase peaks. The *R*-phase transformation induced by pulse lasering of the near equiatomic NiTi thin film is more intensified when crystallographic defects like dislocations are present. Rapid cooling due to the fast solidification can increase these effects (Nam *et al* 2002). A comparison with the previous reports (Sanjabi *et al* 2005), indicates that the

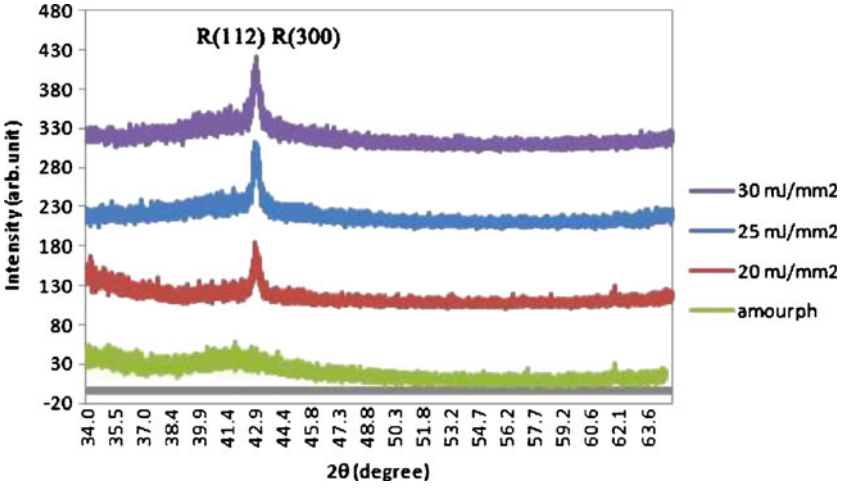

Figure 9. X-ray diffraction spectra of PLA thin film as a function of laser intensity with single pulse irradiation.

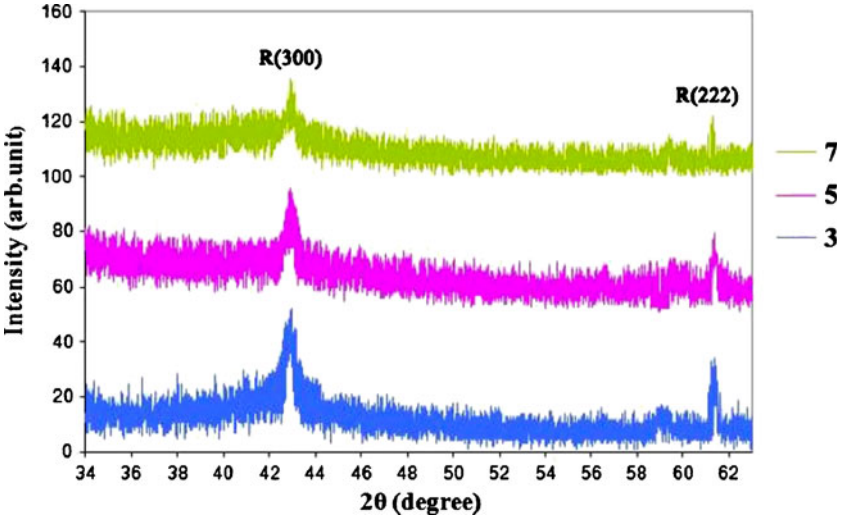

Figure 10. Effect of pulse number on X-ray diffraction spectra of PLA thin film lasered at intensity of 13·2 mJ.

microsecond pulse duration of the Nd:YAG laser creates rapid enough quenching in the spotted layer to form the newly born *R*-phase out of the amorphous phase of the sputtered thin film sample.

The X ray diffraction pattern of the PLA spots lasered at different pulse numbers is shown in figure 10. The crystallized zone indicates larger *R*-phase peaks with greater pulse numbers. According to the literature, peaks observed at $2\theta =$ 42·9 and 61·3 correspond to (300) and (222) planes, respectively (Martins *et al* 2006). Using multipulse PLA leads to the formation of new planes (222) of the *R*-phase which are not seen in the single-pulse PLA (figure 10). However, with 5 and 7 pulses, the peak intensities decrease. This may be the effect of thin film ablation. It is accepted, hence, that the *R*-phase production is more stress related than the thermally influenced regions (Birnbaum *et al* 2009). Increasing of the pulse number of the laser treatment causes more stress which reveals other peaks of the *R*-phases as demonstrated in figure 10.

4. Conclusions

This paper introduces the nanosecond pulse lasering of the amorphous NiTi thin films sputtered on (100) silicon wafers resulting in the stabilization of the rhombohedral structure. Thermal diffusion during the Nd:YAG lasering promotes interaction of nickel, titanium and silicon elements to change the interface chemical composition. Low intensity laser annealing leads to local crystallization of the amorphous phase with no interelemental inclusions. High laser intensity leads, however, to the formation of the rectangle-like inclusions. The nanosecond pulse lasering is preferred to the millisecond in the usual way because of the following advantages: (i) reduction of treatment-time, the film/substrate

interaction and the oxide formation and (ii) more *R*-phase formation. Pulse numbers larger than 7 have, however, the disadvantage of thin film/substrate ablation. Nanosecond pulse lasering gives a better control of the fine film patterns devisable by the small hysteresis of the *R*-phase.

References

Bellouard Y 2008 *Mater. Sci. Eng.* **A481–482** 582

Bellouard Y, Lehnert T, Bidaux J E, Sidler T, Cllavel R and Gothardt R 1999 *Mater. Sci. Eng.* **A273–275** 795

Birnbaum A J, Chung U J, Huang X, Ramirez A G, Im J S and Yao Y L 2008 *Laser microprocessing conference, ICALEO* (Orlando, FL: Laser Institute of America) pp 273–275

Birnbaum J, Chung U J, Huang X, Im J S, Ramirez A G and Yao Y L 2009 *J. Appl. Phys.* **105** 073502·1

Busch J and Johnson A 1991 US patent 5,061,914

Chan P, Chung C and Ng K 2008 *J. Alloys Compd* **449** 148

Clare A T, Chalker P R, Davies S, Sutcliffe C J and Tsopanos S 2008 *J. Mech. Mater. Des.* **4** 181

Fua Y, Du H, Huang W, Zhang S and Hu M 2004 *Sensor Actuator* **A112** 395

Gill J, Ho K and Carmen G 2002 *J. Microelectromech. Sys.* **11** 68

Grummon D, Zhang J and Pence T 1999 *Mater. Sci. Eng. A* **722** 273–275

He Q, Huang W, Gao X and Hon M 2005 *Smart Mater. Struct.* **14** 1320

Ifflander R 2001 *Solid-state lasers for materials processing*, *Fundamental relations and technical realizations* (Berlin: Heidelberg; New York: Springer)

Ishida A, Takei A, Sato M and Miyazaki S 1995 *Mater. Res. Soc. Symp. Proc.* **360** 381

Ivakin E V, Ganjali M, Sukhodolov A and Filippov V 2004 *Quantum Electron.* **34** 294

Kohl M, Dittmann D, Quandt E, Winzek B, Miyazaki S and Allen D 1999 *Mater. Sci. Eng.* **A273–275** 784

Kohl M, Dittmann D, Quandt E and Winzek B 2000 *Sensor Actuator* **83** 214

Krishna V, Bose S and Bandyopadhyay A 2007 *Metall. Mater. Trans.* **A38** 1096

Krishna V, Bose S and Bandyopadhyay A 2009 *J. Biomed. Mater. Res. Part B* **B89** 481

Luskin M and Palmstrom C 2004 *NSF nanoscale science and engineering grantees conference* (Arlington, Virginia: National Science Foundation)

Makino E, Mitsuya T and Shibata T 2000 *Sensor Actuator* **79** 251

Martins R, Schel N, Beckers M, Mahesh K, Silva R J C and Fernandez F 2006 *Appl. Phys.* **A84** 285

Nam T H, Kim J H, Choi M S, Kim Y W, Im H J, Ahn J S and Mitani T 2002 *J. Mater. Sci. Lett.* **21** 685

Ni H, Lee H and Ramirez A G 2005 *J. Mater. Res.* **20** 1728

Sadrnezhaad S, Rezvani E, Sanjabi S and Ziaei Moayed A A 2009 *J. Mater. Sci. Technol.* **25** 135

Sanjabi S, Sadrnezhaad S K, Yates K A and Barber Z H 2005 *Thin Solid Films* **491** 190

Seguin J, Bendahan M, Isalgue A, Esteve-Cano V, Carchano H and Torra V 1999 *Sensor Actuator* **74** 65

Shaw G A and Crone W C 2004 *Mater. Res. Soc. Symp. Proc.* **791** Q7.11.1

Takeuchi S and Shimoyama I 2000 *J. Microelectromech. Sys.* **9** 24

Wang X, Lai A, Vlassak J and Bellouard Y 2004 *Mater. Res. Soc. Symp. Proc.* **795** 275

Wang X, Bellouard Y and Vlassak J J 2005 *Acta Mater.* **53** 4955

Wood A, Sanjabi S, Fu Y, Barber Z and Clyne T W 2008 *Surf. Coat. Technol.* **202** 3115

Xu C, Shi S, Man H, Woo C and Surya C 2006 *J. Mater. Sci.* **41** 1123

Zamponi C, Wuttig M and Quandt E 2007 *Scr. Mater.* **56** 1075

Zanotti C, Giuliania P, Rivaa G, Tuissi A and Chrysanthouc A 2009 *J. Alloys Compd* **473** 231

Zhang J, Botterill N, Roberts C and Grant D 2003 *Thermochim. Acta* **401** 111

Zhan J, Sato M and Ishida A 2006 *Acta Mater.* **54** 1185